Two-dimensional spectroscopic analysis of sulphur group and pyrite transformations in coal coking

Jingbo Chen[1,2], Lechi Zhang[1,2], Xianyou Huang[3,4], Yan Liu[5], Shuxing Qiu[1,3,4], Jianming Wang[5], Sher Farooq[6], Shengfu Zhang[1,2*]

[1]*College of Materials Science and Engineering, Chongqing University, Chongqing 400044, China.*

[2]*Chongqing Key Laboratory of Vanadium–Titanium Metallurgy & Advanced Materials, Chongqing University, Chongqing 400044, China.*

[3]*State Key Laboratory of Vanadium and Titanium Resources Comprehensive Utilization, Panzhihua 617000, China.*

[4]*Panzhihua Iron & Steel Research Institute, Panzhihua 617000, China.*

[5]*Pangang Group Xichang Steel & Vanadium Co. Ltd., Xichang 615000, China.*

[6]*Department of Engineering, Nottingham Trent University, Nottingham NG11 8NS, United Kingdom*

Corresponding author:
Prof. Shengfu Zhang
College of Materials Science and Engineering, Chongqing University
Chongqing 400044
China
Chongqing Key Laboratory of Vanadium–Titanium Metallurgy and Advanced Materials, Chongqing University,
Chongqing 400044
China
Email: zhangsf@cqu.edu.cn (S. Zhang)

Abstract

An accurate description of the sulfur migration process and mechanism is helpful for desulfurization in the coking process, to increase the amount of high–sulfur coking coal and decrease the sulfur content in resultant coke. However, the identified sulfur transformation mechanism in coal pyrolysis is not entirely applicable to the coking process due to variations in atmosphere, temperature and pressure. This work used numerous characterisation techniques in conjunction with experiments to quantitatively evaluate the transformation mechanism of both organic and inorganic sulphur throughout the coking process. The bond–breaking order of functional groups in sulfur during coking was obtained by the Two–Dimensional Correlation Spectroscopy Analysis (2D–COS). The results show that desulfurization in the coking process mainly occurs below 600 °C and 72.8% of sulfur in coal is retained in coke. Among them, FeS_2 and sulfoxide are completely removed while sulfides are reduced by 67.9%. The content of sulfone increases by 46.1% because of the transformation of sulfoxide. Thiophenes, and sulfates increase by 32.5% and 33.9%, respectively, as a result of the inorganic sulfur transformation and secondary reaction of sulfur-containing gases above 500 °C. Through Noda's theorem, the bond–breaking difficulty of sulfur-containing functional groups in the coking process is ordered as follows: Fe–S bond → thiol C–S bond → alkyl sulfide C–S bond → thiol –SH → aliphatic C–S bond → sulfide C–S bond → sulfoxide S=O bond → sulfone, sulfoxide C–S bond. By clarifying the desulfurization characteristics of different forms of sulfur, the desulfurization efficiency in the coking process can be enhanced, which provides a theoretical basis for the extensive utilization of high-sulfur coal.

Keywords: Sulfur transformation; Desulfurization; Coal coking; Pyrite conversion; Sustainable energy; Pollution reduction; Spectroscopic analysis and Two-dimensional correlation spectroscopy.

1. Introduction

Coke plays a fundamental part in the process of blast furnace ironmaking [1], which is produced by pyrolysis of coking coal resources at a high temperature of about 1050 °C [2]. Due to the large output of pig iron in blast furnaces in China, a large amount of coke is consumed every year. With the deficiency of low–sulfur coking coal resources and soaring prices, using cheap high–sulfur coking coal for metallurgical coke production has been accepted and widely applied in some coke ovens. Correspondingly, the coke's residual sulfur increases. When coke with high sulfur is charged into the blast furnace, some adverse effects will appear, such as a coke ratio rise [3], an increase in the sulfur content in pig iron [4] and top gas [5–7], *et al*. Therefore, it is very important to reduce the sulfur content of coke produced in high–sulfur coal blending coking process. High-sulfur coal contains multiple forms of sulfur-containing phases [8], including both inorganic and organic sulfur. Among them, inorganic sulfur primarily exists in the form of pyrite [9], while organic sulfur can be further divided into unstable and relatively stable organic sulfur groups. Sulphur radicals serve as the essential intermediaries for sulphur migration in a two-step reaction mechanism that encapsulates the transformation of sulphur in coal [10]. Specifically, during the coal pyrolysis process, sulfur bonds are initially broken from pyrite or unstable organics, leading to the formation of sulfur radicals. In the subsequent step, these sulfur radicals participate in reactions with other radicals, such as hydrogen radicals generated during coal pyrolysis, and are ultimately expelled as sulfur-containing gases [11].

As previously mentioned, the migration of inorganic sulfur during the coking process primarily involves the transformation of pyrite [9]. During heating, pyrite continuously transforms towards lower sulfur Fe–S phases such as $Fe_{(1-x)}S$ and FeS [12–13]. Setyawati analyzed the evolution of pyrite in Australian coal using TG (Thermogravimetry) and a fixed–bed reactive chamber. The results indicate that pyrite decomposes into pyrrhotite at approximately 927 °C, and beyond this temperature, the pyrrhotite partially dissolves to form iron. [14]. Unlike the pyrite desulfurization that occurs during coal pyrolysis in an inert atmosphere, the desulfurization of pyrite in the coking process faces a more complex chemical environment, which may lead to the formation of phases with various sizes, shapes, and compositions, as well as a difference in transition temperatures. In Gornostayev's research, it was found that pyrite in the coking process almost completely decomposes when the temperature reaches 700 °C [15]. Further heating up to 1400 °C can achieve significant desulfurization of the coke [16]. The desulfurization of pyrite has been proven to have a negative impact on the quality of the produced coke [17]. Unfortunately, in coking process, the interaction between pyrite desulfurization and the coke matrix during coking process has not been clearly explained.

The organic sulfur forms present in coking coal include thiophene, thiosulfate, sulfoxide, mercaptan, and thioether [17]. At lower temperatures, mercaptans, sulfides and disulfides decompose and react with the free hydrogen radicals in the coal, evolving into gaseous forms of sulfur [18]. At the same time, some stable organic sulfur compounds remain in the coke, such as thiophenes and their derivatives [19–20]. Tefera's coal pyrolysis tests in an inert atmosphere showed that thiophene structures break down at temperatures above 900 °C, although thiols and sulphides start to break down at about 200 °C and 350 °C, respectively [21]. Wang [22] discovered that during

the pyrolysis of inertinite–rich coals, thioethers and disulfides can be completely decomposed at 650 °C and 850 °C, respectively. Organic sulfur compounds are fully decomposed at 700 °C. Notably, complex thiophenes do not decompose even at temperatures as high as 1000 °C during pyrolysis. Furthermore, Xu [23] impregnated typical organic sulfur structures from coal onto charcoal and subjected them to pyrolysis. It was found that at lower temperatures (150–350 °C), aliphatic C–S bonds tend to break first, while aromatic C–S bonds are generally more stable. Free radicals with aromatic C–S bonds tend to bind with the coke at lower temperatures instead of producing volatile sulfur compounds. Based on the above studies, a reasonable explanation has been established for the migration of organic sulfur in coal during pyrolysis. However, these results are mostly obtained by the coal pyrolysis experiments in a tubular furnace under an inert atmosphere, which differs from the complex physicochemical environment during the coking process.

Unlike coal pyrolysis in ideal conditions, pretreatment methods employed before coking such as humidification, tamping and crushing effects the migration of sulfur in coal. During the coking process, coal undergoes a state of gas-solid–liquid coexistence in the thermoplastic zone at first [24] and then participates in cross-linking, condensation, and–re-polymerisation reactions [25]. Under a complex atmosphere combined with high temperatures exceeding 1000 °C and elevated pressure, significant changes occur in the thermal transport of harmful sulfur elements. Yang [26] found that the release of sulfur from coal can be enhanced under a coking gas atmosphere. Additionally, moisture in coal has been shown to selectively enhance the breakage ability of C–S bonds, contributing to the formation of sulfur radicals [27]. Chen [28] discovered that H_2S can regenerate stable thiophene structures again by reacting with the organic compounds in the coke at

temperatures higher than 800 °C. According to Tefera's coal pyrolysis experiments conducted in an inert atmosphere, thiophene structures decompose at temperatures exceeding 900 °C, while thiols and sulphides begin to decompose at approximately 200 °C and 350 °C, respectively. Therefore, a fundamental and thorough comprehension of sulfur migration in the coking process is essential and will greatly contribute to improving the performance of coke.

In this study, interruption experiments of coking experiments were carried out at final temperatures ranging from 300 and 1000 °C to recognize the thermal conversion rules of sulfur-containing phases during the coking process qualitatively and quantitatively. The coking products and volatiles during coking processing were analyzed using a combination of techniques, including X-ray Photoelectron Spectroscopy (XPS), X-ray Diffraction (XRD), Scanning Electron Microscope (SEM), Fourier Transform Infrared Spectroscopy (FTIR) combined with 2D–COS and Thermogravimetry–Fourier Transform Infrared Spectroscopy–Mass Spectrometry (TG–FTIR–MS). Through these, the desulfurization characteristics of inorganic and organic sulfur in the coking process, the bond–breaking order of sulfur-containing functional groups, as well as their correlation with sulfur-containing gas emission were described more clearly. This research will offer a theoretical basis for future research on high-sulfur coal utilization and emission control.

2. Materials and methods

Commented [FS1]: Material and methods
This section should consist of the following information.
a)Support each method/technique adopted with literature/ references.
b)Each equation, technique and mathematical expression should be backed by an authentic reference.

2.1 Material

A coking coal from Shanxi province (SX coal) was selected as the experimental coal sample. The proximate and ultimate analysis of the SX coal sample is listed in **Table 1**. SX coal is a high–sulfur coking coal, which has a trace quantity of inorganic sulfur, including pyrite, sulfate, and elevated levels of organic sulfur. For coking experiments, SX coal sample was ground and dried at 110 °C

for 8 h and sieved into particle sizes ranging from 0.15 to 0.25 mm.

2.2 Coking experiments

To study the migration law of coal sulfur in the coking process, coking experiment and its interruption experiment were carried out through crucible coking method. The density, moisture and particle size of coal were controlled at 0.75 t/m^3, 10% and 0.15–0.25 mm, respectively. Firstly, 40 g crushed coking coal was charged into a cylinder-shaped reactor. Then, an asbestos paper was laid on the SX coal sample with a thickness of 0.5–1.0 mm. After that, coke powder with a thickness of 5–10 mm was spread on the asbestos paper, and a metal block was placed on the coke powder. The heating program was structured as follows: the heating rate was set at 5 °C /min before 300 °C, after which it was reduced to 3 °C /min between 300 to 750 °C. When the temperature reached 750 °C, the rate was adjusted to 4.5 °C/min until 1050 °C. The SX coal samples were heated from room temperature to a specific target temperature (300, 400, 500, 600, 700, 800, 900, and 1000 °C, respectively), and then maintained for 2 h to ensure that the desulfurization reaction was fully completed at these temperatures. After cooling, the semi-coke sample was taken out and named SC–300, SC–400, SC–500, SC–600, SC–700, SC–800, SC–900, SC–1000.

2.3 Analytical methods

2.3.1 XPS analysis

The XPS instrumentation (ESCALAB250, America) was employed for the quantitative determination of sulfur's thermal conversion in coal at different interruption temperatures. Before XPS determination, the samples were pre-crushed and filtered to a size of less than 0.074 mm. Al-Kα radiation produced the X-ray source, with a power setting of 200 W. The internal standard calibration was set at 284.6 eV, and the step was set to 0.1 eV. Using the Peakfit software, the spectral characteristics of the sulphur 2p peak were acquired and divided into peaks that

corresponded to FeS2, sulphides, sulphate, sulfoxides, sulfones, and thiophenes. Quantitative analysis of XPS spectra was further carried out to obtain the total sulfur content and sulfur forms distribution of different samples. Due to the mass loss of samples during coking experiments, **Eq. (1)** is used to modify the quantitative data obtained by XPS.

$$S_t' = S_t \times \frac{m_1}{m_0} \quad \textbf{(1)}$$

where, S_t' represents the sulfur content of semi-coke after considering mass loss during the coking process; S_t represents the sulfur content of samples calculated according to XPS spectra; m_0 represents the mass of the original coal sample; m_1 represents the mass of semi-coke after the coking experiment.

2.3.2 XRD and SEM analysis

The samples used in the XRD and SEM analysis were the same as in the XPS analysis. The thermal conversion of inorganic sulfurs was further studied by XRD analysis using a Bruker D8 diffractometer (Rigaku Ultma IV) with Cu–*K*α radiation. The angular scan commenced at a 15° angle and progressed to 90°, moving at a speed of 4° per minute and incrementing at 0.02° per step. The microscopic morphology and element occurrence characteristics of the samples were analyzed by SEM-EDS (Hitachi Regulus 8100, Japan) analysis. Under high–vacuum conditions, secondary electron mode at 30 kV electron beam acceleration voltage was selected for the operation. An energy-dispersive spectrometer was employed to analyze the element content and distribution on the surface of the samples.

2.3.3 FTIR analysis and 2D–COS analysis technique

FTIR measurements of coal and semi–coke samples were performed on an infrared spectrometer (Thermo Scientific Nicolet iS5) to investigate the alteration in sulfur-containing functional groups. Pulverized samples used in XPS analysis continued to be used in FTIR analysis. 32 times scans

were performed for each sample in FTIR sample chamber at ambient temperature. The range of the scanning spectrum was set to 400–4000 cm^{-1} with a spectral resolution of 4.0 cm^{-1}. To thoroughly analyze the transition paths of sulfur-containing functional groups, the FTIR spectrum was extended to two–dimensional domains using the 2D–COS technique. The generalized 2D–COS technique facilitates the analysis of subtle changes in the spectral which may remain concealed in a standard one–dimensional spectrum [29]. It is widely used to study the structural changes in complex systems under external disturbances [30], which has also been proven to be effective in coal pyrolysis researches [31–32]. In this study, 2D–COS transforms one–dimensional variations into two–dimensional domains, producing both a synchronous map and an asynchronous map. Two–dimensional spectra $y(v_i, t)$ and dynamic spectra $\tilde{y}(v_i, t)$ were defined as functions of infrared wave number (v_i) and external temperature (t). The FTIR datasets for the samples were uniformly distributed within the range from T_{min} to T_{max}, as detailed in **Eq. (2**) and **(3)** [33]. The synchronous (Φ) and asynchronous (Ψ) correlation spectra are presented as **Eq. (4)** and **(5)**, The two–dimensional spectral line is analyzed by Noda theorem [41]: When $\Phi(v_1, v_2)$ and $\Psi(v_1, v_2)$ have the same sign, the change of v_1 takes precedence over v_2. Otherwise, the opposite.

$$\tilde{y}(v_i, T) = y(v_i, T) - \bar{y}(v_i) \;\; For\; T_{\min} \le T \le T_{\max} \quad \textbf{(2)}$$

$$\bar{y}(v_i) = \frac{1}{T_{\max} - T_{\min}} \int_{T_{\min}}^{T_{\max}} y(v_i, T) dT \quad \textbf{(3)}$$

$$\Phi(v_1, v_2) = \frac{1}{T_{\max} - T_{\min}} \int_{T_{\min}}^{T_{\max}} \tilde{y}(v_1, T) \cdot \tilde{y}(v_2, T) dT \quad \textbf{(4)}$$

$$\Psi(v_1, v_2) = \frac{1}{T_{\max} - T_{\min}} \int_{T_{\min}}^{T_{\max}} \tilde{y}(v_1, T) \cdot \tilde{z}(v_2, T) dT \quad \textbf{(5)}$$

where, T_{min} and T_{max} are the highest and lowest interruption temperatures, respectively; $\bar{y}(v_i)$ signifies the average spectrum, serving as the reference spectrum as defined in **Eq. (2)**; v_1 and v_2 are the variables of abscissa and ordinate in two-dimensional maps, respectively; $\tilde{y}(v_2, t)$ is the

dynamic spectra, $\tilde{z}(v_2, t)$ is the Hilbert transform of $\tilde{y}(v_2, t)$.

2.3.4 TG–MS–FTIR joint analysis

To further explore the release characteristics of sulfur-containing gases and organic volatiles in the coking process, TG analyzer (SETARAM SETSYS Evolution 16/18, Germany) in conjunction with FTIR (Bruker Tensor 27, Germany) and MS (Pfeiffer OMNI star, Germany) were used to analyze the SX coal sample. To ensure the accuracy of the experiment, a series of stringent testing conditions were implemented. Firstly, the sample mass was meticulously controlled at 10 mg with a margin of error not exceeding 0.002 mg. Besides, an alumina container was chosen for its stability under high temperatures. Then, a high–purity argon atmosphere was utilized to create an inert environment, reducing chemical interference during the heating process. To achieve this, 50 ml/min of argon gas was injected into the system one hour before the experiment. To simulate the coal heating process in real coking environments, the heating range for the experiment was set from 25 to 1000 °C with a heating rate of 10 °C/min, covering a broad spectrum of temperature conditions. Furthermore, the FTIR online monitoring mode was utilized to capture in real-time the spectral features of the volatile fractions released during the decomposition of SX coal. These spectra, spanning a wide range from 4500 to 650 cm^{-1}, provided a wealth of chemical information regarding the migration characteristics of sulfur functional groups.

3. Results and discussion

3.1 Surface chemistry elemental analysis

To understand the migration characteristics at different stages of the coking process [34], Sulfur forms in samples at varying temperatures were examined using XPS. **Fig. 1** displays the fitted curve of the XPS–S_{2p} spectra for six sulfur species in SX coal and semi–coke produced at various temperatures based on the binding energy signals of sulfur compounds [35]. The half-peak breadth

Commented [FS2]: Results and discussion
The results and discussion section is the main part of a research paper, therefore, must need special attention!
a)The main and subheadings in each section should be professional/compressive, don't write the technique name as a heading. Instead, write the output/outcome or main finding out of that technique.
b)Describe the reasons behind the observed trends and discuss your results critically in comparison with the latest published literature wherever it is possible.
c)Each paragraph should consist of 10 to 15 lines and information in each paragraph MUST be supported by some key Numeric Values from the results and should be critically discussed with the literature.
d)Do not just describe only trends without any reference to experimental values. Make, a critical comparison with each other previous studies. Make sure to state values/numbers/percentages and digits etc.
e)If you are mentioning author name then reference/s [Sher et al.,] should be right after the author's name/s not at the end of the sentence or in the paragraph.
f)Do not end a paragraph with any captions such as **Fig. 1 (a)**, **Table 1** or **Eq. (1)** etc. instead cross-reference in the middle of the paragraph.

and peak height related to sulphide sulphur, FeS_2, and sulfoxide drop dramatically as the semi-coke's ultimate temperature rises, and they eventually totally vanish at 700 °C. The modified sulfur content and distribution of sulfur morphology are shown in **Fig. 2**. During the coking process, the absolute sulfur content in the semi–coke samples decrease continuously until 600 °C, after which it changes minimally. Organic sulfur is the predominant sulfur form in SX coal, with sulfide sulfur comprising the highest content (45.1%) and sulfone the lowest (4.0%). Ultimately, 72.8% of the sulfur from the raw coal is retained in the final product, with organic sulfur remaining the primary form, particularly thiophene sulfur (60.8%).

As the temperature increases, sulfur form in different samples undergo significant changes. The levels of sulfides, sulfoxide and pyrite show a continuous declining trend. Ultimately, pyrite and sulfoxide completely vanish. The sulfide content in the product 67.9% lower than that of raw coal. This decrease can be ascribed to the breakdown of mercaptans, sulfides and other volatile organic sulfur compounds. In contrast, the content of sulfone initially increased before declining, showing an increase of 68.42% compared with the coal. The peak of sulfone content appears at 600 °C, which is twice that of raw coal. This increase is due to the conversion of sulfoxide to more heat–stable sulfone, facilitated by oxygen-containing groups in coke within this temperature range. Once the temperature exceeds 600 °C, sulfone begins to decompose gradually, eventually decreasing to 73.54% of its peak content. Additionally, the contents of sulfate and thiophene during this process both initially decrease and then increase, with increases of 32.5% and 33.9% respectively compared to their levels in the raw coal. From 400 to 1000 °C, oxygen-containing groups react with inorganic sulfides in the coke, leading to a continuous increase in sulfate content [36]. Thiophene sulfur slightly decreases before 500 °C, as the thiophene groups at the end of the branched chain separate into free organic fragments due to the breakage of unstable C–S bond. In

the high–temperature environment above 500 °C, the sulfur gases released will engage in secondary reactions with the coke matrix, resulting in the formation of new thiophene phases [37]. This process contributes to the overall increase in sulfur content in the coking process.

3.2 Crystalline structure and surface topography analysis

It's difficult to definitively analyze the migration of inorganic sulfur in the coking process solely based on XPS data. Thus, XRD analysis coupled with SEM analysis was used to further study the conversion rules of inorganic sulfur in coal coking process. In addition, its impact on coke production was also further explored. **Fig. 3** displays the XRD patterns of coal and semi–coke samples subjected to pyrolysis at various temperatures. Native inorganic sulfur in SX coal consists of FeS_2 and $Fe_2(SO_4)_3$. Among them, FeS_2 starts to decompose at temperatures above 300 °C. At pyrolysis temperatures exceeding 700 °C, $Fe_{(1-x)}S$, FeS_2 and $Fe_2(SO_4)_3$ disappear completely. FeS begins to form when the coking temperature rises to 1000 °C. Unlike the thermal decomposition pattern of FeS_2 in coal reported by Zhou [38] and Zhao [39], the appearance temperature of FeS in coking process is significantly higher. The discrepancy is attributed to the insufficient presence of hydrogen and oxygen free radicals in the coking process, which limits the reaction with FeS_2 and results in a lower sulfur removal rate.

SEM was employed to further investigate sulfur-containing minerals in coal and semi–coke samples. As shown in **Fig. 4(a)**, the results indicate that the FeS_2 aggregates in SX coal are mainly embedded within the coal particles or spherically agglomerated around the coal particle boundaries. **Fig. 4(b)** shows the overlapping distribution of sulfur and iron elements in SC–500, indicating that Fe–S phase minerals still exist as aggregates within the coke matrix during the coking process. The SEM image of SC–700 presented in **Fig. 4(c)** reveals that the Fe–S phase in the coke is

277 gradually desulfurizing. As this process occurs, the Fe–S phase continuously transitions to a low
278 sulfur phase, accompanied by the formation of new Fe–O–S phases. Further, as shown in **Fig. 4(d)**,
279 when the temperature rises to 1000 °C, some aggregates of the Fe–S phase completely disappear.
280 Based on the aforementioned analysis, the desulfurization of FeS_2 under coking conditions can be
281 summarized in the following steps. Initially, in the thermoplastic process, Fe–S phase minerals
282 bind with the coke matrix. At the same time, FeS_2 starts desulfurization, transitioning towards $Fe_{(1-x)}S$.
283 During the heating process, desulfurization initiates from the fringe of the coke matrix and
284 proceeds inward. The Fe–S phase transitions from $Fe_{(1-x)}S$ to low sulfur Fe–S phases (FeS).
285 Following the completion of the coking process, some of the Fe–S phases are fully desulfurized,
286 resulting in the formation of spherical iron elemental. Additionally, the desulfurization process
287 introduces pores and defects into the coke, which may lead to a reduction in its mechanical
288 properties [40].

289 **3.3 Chemical composition and dynamic molecular interactions analysis**

290 To gain a deeper understanding of which sulfur-containing compounds are easily removed during
291 the coking process, a study was conducted to investigate the decomposition order of trace sulfur-
292 containing functional groups in semi-coke during heating. To analyze these changes more
293 intuitively, 2D–COS was used to enhance the FTIR spectra as shown in **Fig. 5(a)**. As shown in **Fig.**
294 **5(b)–(h)**, since both synchronous and asynchronous maps have the characteristic of diagonal–
295 centred symmetry, the measurement above the diagonal of the synchronous spectrum is flipped
296 diagonally and covers the part below the diagonal of the asynchronous spectrum. Referring to the
297 peaks observed in the synchronous and asynchronous spectrum shown in **Fig. 5(b)–(h)**, the
298 identification and designation of each cross–peak as detailed in **Table 2** can be derived. From **Fig.**
299 **5(b)**, the sequential change order of the peaks can be determined by Noda theorem as follows:

425→475→535→800→750→870 cm^{-1} during the heating interval from room temperature up to 400 °C. Correspondingly, the sequence of changes in sulfur-containing functional groups [38], from first to last, is as follows: FeS_2 → Thiol –SH bond → thioether C–S bond → Thiol C–S bond → Thiol S–S bond → aliphatic C–S bond. It can be observed that the sulfur from FeS_2 is the first to be removed, followed by an alternating decomposition of thiol and thioether functional groups. This suggests that the transformation temperatures of unstable sulfur-containing functional groups are very close below 400 °C.

It can be deduced from **Fig. 5(c)** that the corresponding sequence of changes in sulfur-containing functional groups within the temperature range of 300–500 °C is: FeS_2 → Thiol –SH bond → Thiol C–S bond → Thiol S–S bond → aliphatic C–S bond → thioether C–S bond. Notably, there are significant changes in aliphatic sulfur at 870 cm^{-1}, while the corresponding absorption band of aromatic sulfur (630–700 cm^{-1}) undergoes virtually no changes. This observation aligns with the pattern discovered by Xu L [23], indicating that aromatic C–S bonds have higher decomposition temperatures compared to aliphatic C–S bonds. The higher stability of aromatic C–S bonds can be attributed to the electron delocalization in aromatic systems, which reinforces the C–S bond and thus necessitates more energy (higher temperature) to break. From **Fig. 5(d)**, the change order of sulfur-containing functional group in the temperature range of 400–600 °C is as follows: FeS_2→Thioether C–S bond →S=O bond →sulfoxide C–S bond. It can be found that the peak position changes corresponding to Thiol S–S bond, –SH bond and C–S bond basically disappear above 500 °C. This indicates that the thiol, as the most unstable organic sulfide, has been completely removed before 500 °C. In combination with the spectral feature in **Fig. 5(e)**, it is apparent that the principal transformation occurring at 500–600 °C is related to sulfoxide and

sulfone functional groups. The synchronous and asynchronous spectra exhibited in **Fig. 5(f)–(h)** all display analogous patterns, with changes occurring in the following sequence: FeS_2→S=O bond →sulfoxide C–S bond. Due to the influence of the changes of C–O–C and–OH of phenols, alcohols, ethers, and lipids in the 860–1040 cm^{-1} band, the peak intensity has a high presence on the diagonal of the synchronous line, and the relative intensity of changes in sulfur-containing functional groups within this temperature range cannot be accurately estimated.

In the coking experiment, to mimic the prolonged heating duration experienced in the coke oven, isothermal conditions were maintained at the final temperature for 2 h. Hence, the decomposition of sulfur-containing phases is almost completely over in all temperature ranges. The intensity of the functional groups corresponding to each peak position affected by temperature can be determined by the value of the intersection point of the diagonal line of the synchronous correlation line. As shown in **Table 2**, thiol and thioether are the majority of organic sulfur compounds in SX coal. By comparing the intensities of the synchronous spectrum peaks in the ranges of RT–400 °C, 300–500 °C and 400–600 °C, it becomes evident that there are prominent variations in the distinct peaks of organic sulfur compounds in the ranges of RT–400 °C, while these peak values vary little in the ranges of 300–500 °C and 400–600 °C, indicating that the decomposition of organic sulfur compounds in the coking process is predominantly concentrated before 300 °C. In addition, FeS_2 sulfur continues to be continuously removed before 600 °C, which aligns with the patterns discovered in **section 3.2**, corroborating that the removal of FeS_2 sulfur in the coking process is a slow and continuous procedure [42].

3.4 Thermal decomposition and volatiles evolution curves

The removal of sulfur in the coking process basically depends on the emission of sulfur-containing

346 gases and low–molecule compounds [44–45]. TG–DTG analysis presented in **Fig. 6(a)** shows that
347 the weight loss rate fluctuated with temperature, leading to two distinct peaks in the DTG curves.
348 The first peak in weight loss for SX coal is attributed to the removal of water, while the second
349 peak corresponds to the rapid escape of volatile matter. **Fig. 6(b)** summarizes the time–evolved
350 flow flowrates of five selected products during the pyrolysis process of the SX coal sample. The
351 mass–to–charge ratios for the different gases are as follows: CS_2 (m/z=76), H_2S(m/z=34),
352 SO_2(m/z=64), C_4H_4S(m/z=84), COS(m/z=60). In the coking process, SO_2 begins to be emitted at
353 110 °C., peaks at 535 °C, and continues to be generated during subsequent heating. H_2S generation
354 occurs at higher temperature, exhibiting two obvious emission peaks at 500 °C and 1000 °C. CS_2
355 and C_4H_4S show similar emission ranges (300–540 °C), with maximum emission temperatures
356 both at 480 °C. The release of COS starts at 480 °C and concludes at 550 °C, peaking at 515 °C.
357 Similar to other volatiles, sulfur-containing petrol emissions are concentrated in the thermoplastic
358 stage of the coking process, as evidenced by the temperature range for these emissions matching
359 the time of rapid weight loss seen during coal pyrolysis. **Fig. 7** illustrates the three–dimensional
360 FTIR diagrams of volatile products produced from the pyrolysis of SX coal. The acquired
361 wavenumber, absorbance and temperature data facilitate the identification of evolved volatiles
362 through their distinctive absorption bands. The stretching vibration peak of S=O is located at 1300
363 cm^{-1} [46] between 400 and 600 °C, which represents the release of SO_2 [47]. This observation aligns
364 with the temperature range in which sulfoxide sulfur content decreases as observed in Section 3.3.
365 It is evident that most of the sulfoxide sulphur in the SX coal is oxidised to sulfone during the
366 coking process, with a tiny amount escaping as minute chemical molecules [48]. The peaks
367 observed before 650 cm^{-1} correspond to the C–S stretching vibrations of thiols. The peaks near
368 1400 cm^{-1} correspond to the release of –OH in the coke matrix.

A clear linear correlation exists between the intensity of C–S and –OH release and the pyrolysis temperature, indicating that coke releases more hydrogen and oxygen free radicals at high temperatures. In the coking process, the desulfurization of organic sulfur occurs continuously and synchronously with the release of –OH groups, which have a strong affinity for sulfur radicals [49]. This suggests that the continued decomposition of hydrogen-containing functional groups can provide hydrogen radicals for the desulfurization in the coking process. Additionally, it also shows that coals with a higher content of –OH groups will exhibit enhanced desulfurization performance in the coking process. The information obtained from the above analysis can be summarized in **Fig. 8**. The sulfur sources of SO_2 and H_2S released at temperatures below 300 °C primarily originate from the sulfur-containing groups in thiols. The subsequent increase in SO_2 and H_2S emission above 300 °C results from (1) the reaction of sulfur in FeS_2 with hydrogen–containing groups and oxygen-containing groups, (2) the breakage of aromatic C–S bonds, (3) the decomposition of sulfates, specifically $CaSO_4$ and $Fe_2(SO_4)_3$. Equally important, the emission ranges of CS_2 and C_4H_4S coincide with the decomposition ranges of aliphatic sulfur and thioether sulfur. The massive breakage of unstable S–S and C–S bonds leads to the concentrated emission of CS_2 and C_4H_4S, which is barely related to the sulfur free radicals produced by the inorganic sulfur.

4. Conclusion

The migration patterns and characteristics of sulfur forms during the coking process of coal were investigated using XPS, XRD and SEM-EDS technologies. The FTIR spectra were analysed using the 2D–COS approach, which yielded a more precise evaluation of the alterations in the functional groups in coal that contain trace sulphur. Furthermore, the combined TG–FTIR–MS approach was

applied to investigate the volatile matter in coal's emission properties. The following conclusions were drawn:

- During the coking process, sulfoxides continue to oxidize to sulfone until complete oxidation at 700 °C. Sulfides continue to decompose below 600 °C. Thiophene decreases below 500 °C and rises again above 500 °C due to the transformation of inorganic sulfur. Due to the secondary reaction of sulfur-containing gases, the sulfate content increases above 500 °C.
- The FeS_2 in coking coal distributed on coal surface and within the gaps binds with the coke matrix after the thermoplastic process. As the heating goes on, the Fe–S phase transitions from $Fe_{(1-x)}S$ to low sulfur Fe–S phases (FeS). Ultimately, part of the FeS_2 transforms into elemental iron, creating pores in coke. The decomposition of FeS_2 is more difficult in the coking process due to the lack of hydrogen and oxygen free radicals.
- The changes order of sulfur-containing functional groups in the coking process is as follows: Fe–S bond → thiol C–S bond → alkyl sulfide C–S bond → thiol –SH → aliphatic C–S bond → thioether C–S bond → sulfoxide S=O bond → sulfone, sulfoxide C–S bond.
- The decomposition of most sulfur-containing functional groups around 500 °C leads to the release of H_2S, CS_2, SO_2, C_4H_4S, COS and low–molecular sulfur-containing organic compounds. The continuous emission of H_2S and SO_2 can primarily be attributed to the pyrolysis of FeS_2 and sulfates. The emission ranges of CS_2 and C_4H_4S coincide with the decomposition ranges of aliphatic and thioether.

Acknowledgement

The work is supported by the National Natural Science Foundation of China (Project No. 52074055 & 52104323), and the Chongqing Talent Program (Project No. cstc2021ycjhbgzxm0108

415 & CQYC201905039). The authors are also grateful to the International Society of Engineering
416 Science and Technology (ISEST), UK.

417 **Abbreviations**

418 2D–COS, Two–Dimensional Correlation Spectroscopy Analysis; TG, Thermogravimetric; XPS,
419 X–ray Photoelectron Spectroscopy; XRD, X–ray Diffraction; SEM, Scanning Electron
420 Microscope; FTIR, Fourier Transform Infrared Spectroscopy; TG–FTIR–MS, Thermogravimetry
421 – Fourier Transform Infrared Spectroscopy – Mass Spectrometry; SX coal, A coking coal from
422 Shanxi province.

423

References

[1] Zhang, H.; Bai, J.; Li, W.; Cheng, F. Comprehensive evaluation of inherent mineral composition and carbon structure parameters on CO_2 reactivity of metallurgical coke. Fuel 2019, 235: 647–657.

[2] Li, K.; Khanna, R.; Zhang, J.; Liu, Z.; Sahajwalla, V.; Yang, T.; Kong, D. The evolution of structural order, microstructure and mineral matter of metallurgical coke in a blast furnace: A review. Fuel 2014, 133: 194–215.

[3] Shen, Y.; Wang, M.; Wu, Y.; Hu, Y.; Kong, J.; Duan, X.; Wang, Y.; Chang, L.; Bao, W. Role of Gas Coal in Directional Regulation of Sulfur during Coal-Blending Coking of High Organic-Sulfur Coking Coal. Energy & Fuels 2020, 34(3): 2757–2764.

[4] Shen, Y.; Hu, Y.; Wang, M.; Bao, W.; Chang, L.; Xie, K. Speciation and thermal transformation of sulfur forms in high–sulfur coal and its utilization in coal–blending coking process: A review. Chinese J Chem Eng 2021, 35: 70–82.

[5] Cui, L.; Liu, M.; Yuan, X.; Wang, Q.; Ma, Q.; Wang, P.; Hong, J.; Liu, H. Environmental and economic impact assessment of three sintering flue gas treatment technologies in the iron and steel industry. J Clean Prod 2021, 311: 127703.

[6] Zeng, B.; Li, H.; Huang, T.; Liu, C.; Yue, H.; Liang, B. Kinetic study on the sulfidation and regeneration of manganese–based regenerable sorbent for high temperature H_2S removal. Ind Eng Chem Res 2015, 54(4): 1179–1188.

[7] Lee, W.; Lee, Y. Internal gas pressure characteristics generated during coal carbonization in a coke oven. Energy & Fuels 2001, 15(3): 618–623.

[8] Liu, J.; Yang, X.; Jiang, Y.; Zhang, H.; Jiang, X.; Jiang, X. Chemical Properties of Superfine Pulverized Coal Particles. Part 4. Sulfur Speciation by X-ray Absorption Near-Edge Structure Spectroscopy. Energy & Fuels 2020, 34(11): 13686–13697.

[9] Zhang, Z.; Wei, X.; Yan, G.; Guo, J.; Zhao, P.; Yang, F.; Zhao, H.; Zhang, B. Formation of pyrite in the process of fine coal desulfurization by microwave enhanced magnetic separation. Int J Coal Prep Util 2023, 43(3): 484–501.

[10] Cai, S.; Zhang, S.; Wei, Y.; Sher, F.; Wen, L.; Xu, J.; Dang, J.; Hu, L. A novel method for removing organic sulfur from high–sulfur coal: Migration of organic sulfur during microwave treatment with $NaOH–H_2O_2$. Fuel 2021, 289: 119800.

[11] Tang, Y.; Sun, Y.; Wang, X.; Yan, L.; Shi, Q.; Ni, H.; Li, W.; Li, X.; Finkelman, R.; Pang, X. Composition and Structure of the Sulfur-Containing Compounds in the Extracts from the Chinese High-Organic-Sulfur Coals. Energy & Fuels 2020, 34(9): 10666–10675.

[12] Kuang, Y.; Cai, S.; Zhang, L.; Zhang, S. Transformation behavior of FeS_2 during microwave desulfurization from coal: Phase and structural change of Fe–S compounds. Fuel 2022, 316: 123284.

[13] Wu, Y.; Zhang, S.; Cai, S.; Xiao, X.; Yin, C.; Xu, J.; Qiu, S.; Yu, W.; Hu, M.; Wen, L. Transformation of organic sulfur and its functional groups in nantong and laigang coal under microwave irradiation. J Comput Chem 2019, 40(31): 2749–2760.

[14] Yani, S.; Zhang, D. An experimental study into pyrite transformation during pyrolysis of Australian lignite samples. Fuel 2010, 89(7): 1700–1708.

[15] Gornostayev, S.; Heikkinen, E.; Heino, J.; Fabritius, T. Occurrence and behavior of sulfur‐bearing minerals in metallurgical coke. Steel Res Int 2018, 89(4): 1700470.

[16] Gornostayev, S.; Härkki, J.; Kerkkonen, O. Transformations of pyrite during formation of metallurgical coke. Fuel 2009, 88(10): 2032–2036.

[17] Huang, F.; Xin, S.; Mi, T.; Zhang, L. Study of pyrite transformation during coal samples heated in CO_2 atmosphere. Fuel 2021, 292: 120269.

[18] Xiao, J.; Deng, S.; Zhong, Q.; Ye, Shao. Effect of sulfur impurity on coke reactivity and its mechanism. Transactions of Nonferrous Metals Society of China 2014, 24: 3702–3709.

[19] Yin, C.; Zhang, S.; Wang, J.; Sher, F.; Cai, S.; Xu, J.; Hu, M.; Wen, L. Chemical thermodynamics and kinetics of thiophenic sulfur removed from coal by microwave: a density functional theory study. J Sustain Metall 2021, 7(3): 1379–1392.

[20] Meng, N.; Jiang, D.; Liu, Y.; Gao, Z.; Cao, Y.; Zhang, J.; Gu, J.; Han, Y. Sulfur transformation in coal during supercritical water gasification. Fuel 2016, 186: 394–404.

[21] Telfer, M.; Zhang, D. The influence of water–soluble and acid–soluble inorganic matter on sulfur transformations during pyrolysis of low–rank coals. Fuel 2001, 80(14): 2085–2098.

[22] Wang, M.; Hu, Y.; Wang, J.; Chang, L.; Wang, H. Transformation of sulfur during pyrolysis of inertinite–rich coals and correlation with their characteristics. J Anal Appl Pyrol 2013, 104: 585–592.

[23] Xu, L.; Yang, J.; Li, Y.; Liu, Z. Behavior of organic sulfur model compounds in pyrolysis under coal–like environment. Fuel Processing Technology 2004, 85(8): 1013–1024.

[24] Wu, J.; Liu, J.; Yuan, S.; Zhang, X.; Liu, Y.; Wang, Z.; Zhou, J. Sulfur Transformation during Hydrothermal Dewatering of Low Rank Coal. Energy & Fuels 2015, 29(10): 6586–6592.

[25] Lee, S.; Brooks, B.; Chen, Y.; Hockings, K.; Yu, J.; Tahmasebi, A. Mechanistic study of plastic layer permeability during coking of Australian metallurgical coals. Fuel 2023, 331: 125739.

[26] Yang, N.; Guo, H.; Liu, F.; Zhang, H.; Hu, Y.; Hu, R. Effects of atmospheres on sulfur release and its transformation behavior during coal thermolysis. Fuel 2018, 215(1): 446–453.

[27] Yu, J.; Tahmasebi, A.; Han, Y.; Yin, F.; Li, X. A review on water in low rank coals: The existence, interaction with coal structure and effects on coal utilization. Fuel Processing Technology 2013, 106: 9–20.

[28] Chen, L.; Bhattacharya, S. Sulfur Emission from Victorian Brown Coal Under Pyrolysis, Oxy–Fuel Combustion and Gasification Conditions. Environmental Science & Technology 2013, 47(3): 1729–1734.

[29] Ni, Z.; Song, Z.; Bi, H.; Jiang, C.; Sun, H.; Qiu, Z.; He, L.; Lin, Q. The effect of cellulose on the combustion characteristics of coal slime: TG–FTIR, principal component analysis, and 2D–COS. Fuel 2023, 333: 126310.

[30] Peng, S.; Wang, F.; Wei, D.; Wang, C.; Ma, H.; Du, Y. Application of FTIR two–dimensional correlation spectroscopy (2D–COS) analysis in characterizing environmental behaviors of microplastics: A systematic review. Journal of Environmental Sciences 2025, 147: 200–216.

[31] Bodappa, N.; Stepan, S.; Smith, R. Analysis of solid–state reaction mechanisms with two–dimensional fourier transform infrared correlation spectroscopy. Inorganic Chemistry 2021, 60: 2304–2314.

[32] Fudge, A.; Wilkinson, K.; Ristic R; Cozzolino, D. Synchronous two–dimensional MIR correlation spectroscopy (2D–COS) as a novel method for screening smoke tainted wine. Food chemistry 2013, 139(1): 115–119.

[33] Li, T.; Song, F.; Bai, Y.; Wu, F.; Ruan, M.; Cao, Y.; Zhou, L.; Sun, F. Real–Time Emission, Chemical Properties, and Dynamic Evolution Mechanism of Volatile Organic Compounds during Co–Pyrolysis of Rice Straw and Semi–Bituminous Coal. ACS ES & T Engineering 2023, 3(5): 690–705.

[34] Lee, S.; Yu, J.; Mahoney, M.; Tahmasebi, A.; Stanger, R.; Wall, T.; Lucas, J. In–situ study of plastic layers during coking of six Australian coking coals using a lab–scale coke oven. Fuel Processing Technology 2019, 188: 51–59.

[35] Liu, F.; Li, W.; Chen, H.; Li, B. Uneven distribution of sulfurs and their transformation during coal pyrolysis. Fuel 2007, 86(3): 360–366.

[36] Yankovsky, S.; Tolokol, A.; Misyukova, A.; Kuznetsov, G. On the Effect of the distances between coal and wood particles during Their Joint Pyrolysis on Sulfur Oxides Formation. Energies 2021, 14(24): 8321.

[37] Hou, J.; Ma, Y.; Li, S.; Shi, J.; He, L.; Li, J. Transformation of sulfur and nitrogen during Shenmu coal pyrolysis. Fuel 2018, 231: 134–144.

[38] Wang, M.; Gao, J.; Xu, J.; Du, Q.; Zhang, Y. Effect of H_2O on the Transformation of Sulfur during Demineralized Coal Pyrolysis: Molecular Dynamics Simulation Using ReaxFF. Energy & Fuels 2021, 35(3): 2379–2390.

[39] Zhao, H.; Bai, Z.; Bai, J.; Guo, Z.; Kong, L.; Li, W. Effect of coal particle size on distribution and thermal behavior of pyrite during pyrolysis. Fuel 2015, 148: 145–151.

[40] Zou, C.; Yu, N.; Ma, C.; Li, B.; Liu, S. Effects of pyrolysis temperature and atmosphere on grinding properties of semicoke prepared from Shenmu low–rank coal. J Anal Appl Pyrol 2023, 173: 106059.

[41] Hur, J.; Jung, K.; Jung, Y. Characterization of spectral responses of humic substances upon UV irradiation using two–dimensional correlation spectroscopy. Water Research 2011, 45(9): 2965–2974.

[42] Zheng, Z.; You, Y.; Guo, J.; Li, G.; You, Z.; Lv, X. Pyrolysis Behavior of Pyrite under a CO–H_2 Atmosphere. ACS omega 2022, 7(33): 29116–29124.

[43] Yang, Y.; Tao, X.; Kang, X.; He, H.; Xu, N.; Tang, L.; Luo, L. Effects of microwave/HAc–H_2O_2 desulfurization on properties of Gedui high–sulfur coal. Fuel Processing Technology 2016, 143: 176–184.

[44] Yu, X.; Yu, D.; Yu, G.; Liu, F.; Han, J.; Wu, J.; Xu, M. Temperature–resolved evolution and speciation of sulfur during pyrolysis of a high–sulfur petroleum coke. Fuel 2021, 295: 120609.

[45] Irfan, M.; Usman, M.; Kusakabe K. Coal gasification in CO_2 atmosphere and its kinetics since 1948: A brief review. Energy 2011, 36(1): 12–40.

[46] Chen, C.; Tang, Y.; Guo, X. Comparison of structural characteristics of high–organic–sulfur and low–organic–sulfur coal of various ranks based on FTIR and Raman spectroscopy. Fuel 2022, 310: 122362.

[47] Tang, L.; Chen, S.; Gui, D.; Zhu, X.; He, H.; Tao, X. Effect of removal organic sulfur from coal macromolecular on the properties of high organic sulfur coal. Fuel 2020, 259: 116264.

552 [48] Wang, Q.; Xuan, Y.; Liu, H.; Li, X.; Chi, M. Gaseous emission and thermal analysis during
553 co–combustion of oil shale semi–coke and sawdust using TG–FTIR. Oil Shale 2015, 32(4):
554 356.
555 [49] Oudghiri, F.; Allali, N.; Quiroga, J.; Rodriguez, M. TG–FTIR analysis on pyrolysis and
556 combustion of marine sediment. Infrared Physics & Technology 2016, 78: 268–274.
557

List of Tables

Table 1. Proximate and ultimate analysis of coking coal.

Sample	Proximate analysis (%)				Ultimate analysis (%)				Sulfur forms in total sulfur (%)		
	M_{ad}	A_{ad}	V_{ad}	FC_{ad}	C_d	H_d	N_d	S_d	S_s	S_p	S_o
SX coal	1.72	9.88	21.90	66.50	78.50	3.78	1.35	1.95	6.21	8.00	85.79

M: Moisture; *A*: Ash; *V*: Volatile; *FC*: Fixed carbon; S_s: Sulfate sulfur; S_p: Pyritic sulfur; S_o: Organic sulfur; ad: Air dry basis; d: Dry basis.

565

566 **Table 2.** Sign of each cross–peak in synchronous (outside brackets) and asynchronous maps
567 (inside brackets) of coal and semi–coke at different temperature ranges.

RT–400 °C		sign[α]					
Position (cm^{-1})	**assignment**	**425**	**475**	**535**	**750**	**800**	**870**
425	FeS_2	17.85					
475	–SH bond bending vibration	+(+)	56.96				
535	thioether C–S bond stretching vibration	+(+)	+(+)	101.6			
750	S–S bond bending vibration	+(+)	+(+)	+(+)	88.77		
800	Thiol C–S bond stretching vibration	+(+)	+(+)	+(+)	+(–)	73.23	
870	Aliphatic C–S bond stretching vibration	+(+)	+(+)	+(+)	+(+)	+(+)	72.31
300–500 °C		**sign[α]**					
Position(cm^{-1})	**Assignment**	**425**	**475**	**535**	**750**	**800**	**870**
425	FeS_2	7.21					
475	–SH bond bending vibration	+(+)	11.28				
535	thioether C–S bond stretching vibration	+(+)	+(+)	21.81			
750	S–S bond bending vibration	+(+)	+(+)	+(–)	23.18		
800	Thiol C–S bond stretching vibration	+(+)	+(+)	+(–)	+(–)	19.45	
870	Aliphatic C–S bond stretching vibration	+(+)	+(+)	+(–)	+(+)	+(+)	19.94
400–600 °C		**sign[α]**					
Position(cm^{-1})	**Assignment**	**425**	**535**	**735**	**780**	**950**	
425	FeS_2	4.21					
535	thioether C–S bond stretching vibration	+(+)	13.15				
735	Substituted aromatics–CH stretching vibration at each position	+(+)	+(+)	14.30			
780	Sulfoxide, sulfone C–S bond stretching vibration	+(+)	+(+)	+(+)	11.85		
950	S = O bond stretching vibration	+(+)	+(+)	+(–)	+(–)	8.89	

500–1000 °C		sign[α]		
Position(cm^{-1})	**Assignment**	**425**	**820**	**950**
425	FeS_2			
820	Sulfoxide, sulfone C–S bond stretching vibration	–(–)		
950	S=O bond stretching vibration	–(–)	+(–)	

sign[α] were obtained in the lower–right corner of maps: +, positive; –, negative.

List of Figures

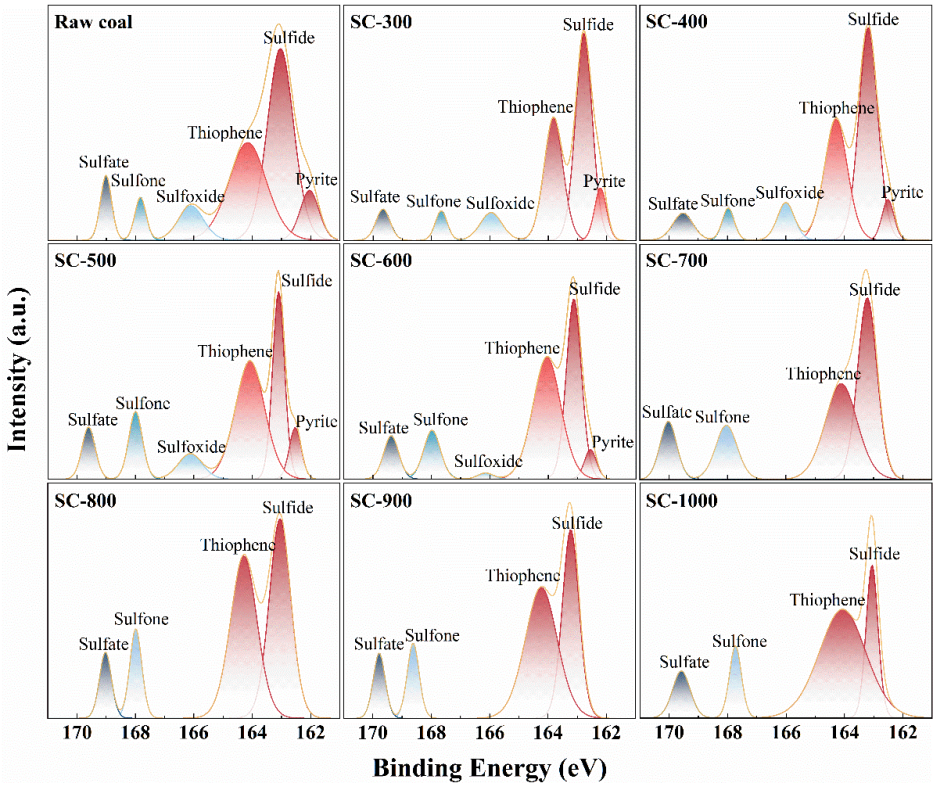

Fig. 1. XPS–S_{2p} spectra of sulfur form in the produced semi–coke at different interruption temperatures during cooking.

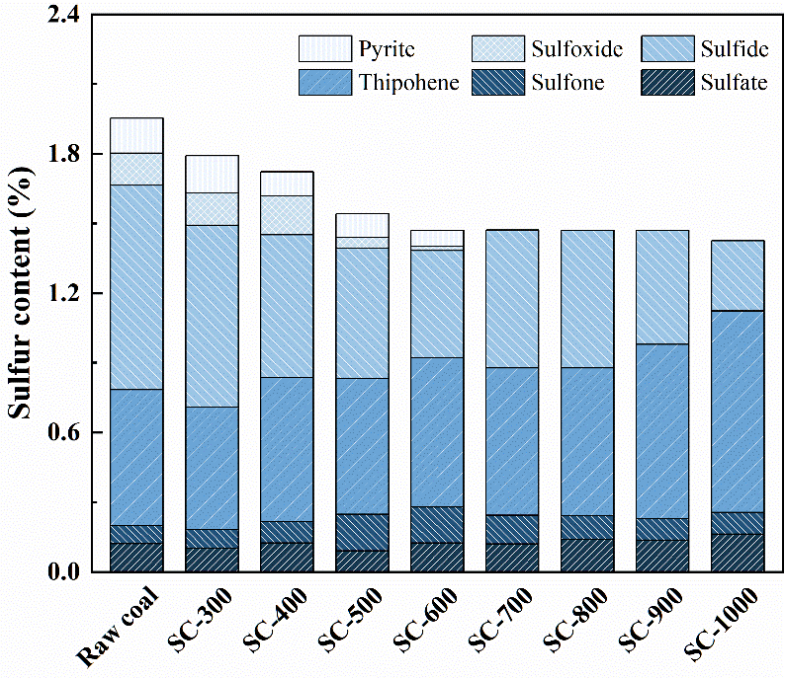

Fig. 2. Distributions of sulfur forms in the produced semi–coke at different interruption temperatures during cooking.

588
589
590
591

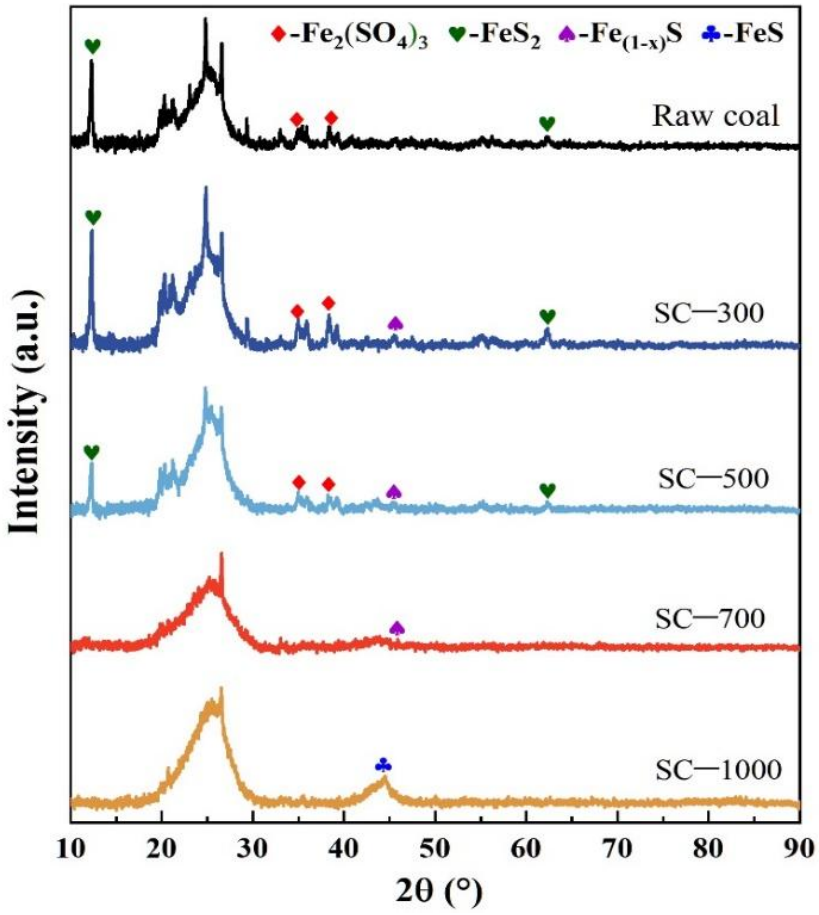

592

593 **Fig. 3.** XRD spectra of inorganic sulfur in the produced semi–coke at different interruption
594 temperatures during cooking.

595

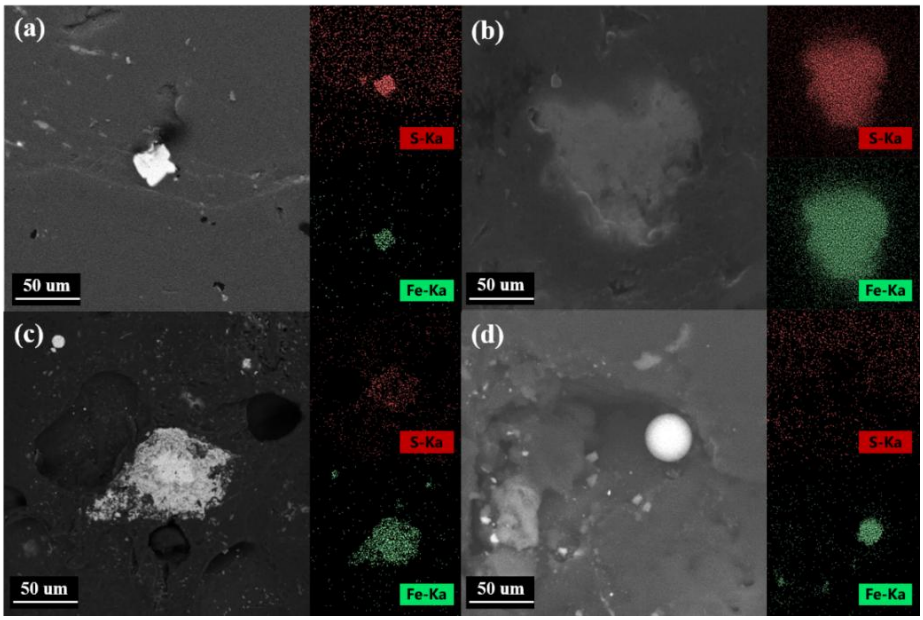

Fig. 4. SEM images of Fe–S phase distribution in the produced semi–coke at different interruption temperatures during coking; (a) Raw coal, (b) 500 °C, (c) 700 °C and (d) 1000 °C.

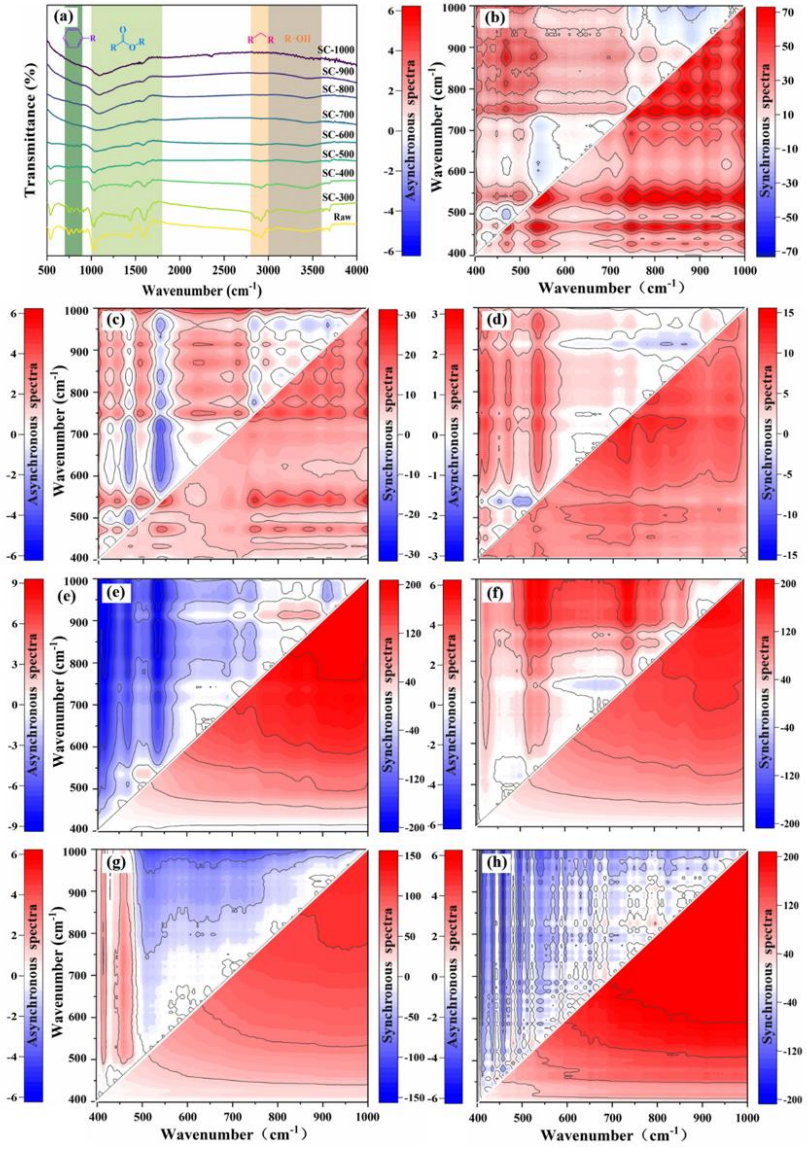

Fig. 5. FTIR spectra and generalized 2D–FTIR–COS synchronous and asynchronous maps of samples at different interruption temperatures during the coking process; (a) FTIR spectra, (b) RT–400 °C, (c) 300–500 °C, (d) 400–600 °C, (e) 500–700 °C, (f) 600–800 °C, (g) 700–900 °C and (h) 800–1000 °C.

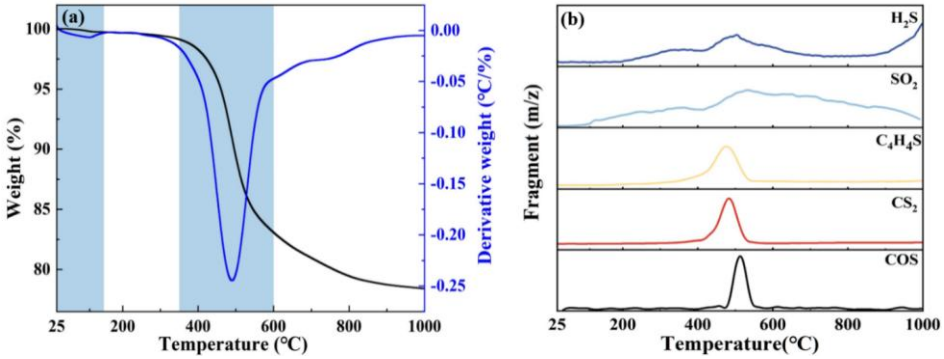

Fig. 6. (a) TG/DTG curves of coal at a heating rate of 10 °C/min and (b) Evolution curves of H_2S, SO_2, C_4H_4S, CS_2 and COS during coal pyrolysis.

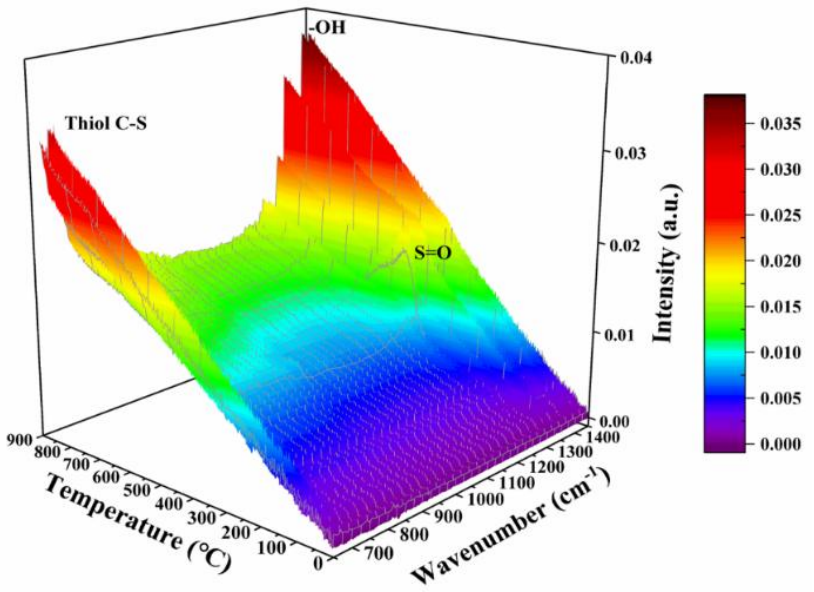

Fig. 7. Three–dimensional FTIR (1500–650 cm^{-1}) spectra of volatile results from coal pyrolysis.

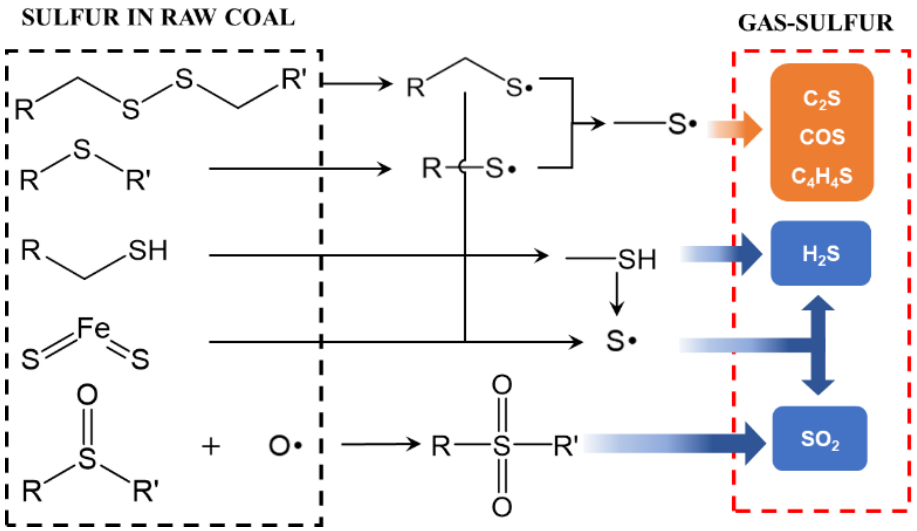

Fig. 8. Mechanisms of sulfur-containing gas escape resulting from pyrolysis of sulfur phase in the coking process.